

# Structural Analysis of Soot Agglomerates<sup>†</sup>

R. J. Samson,<sup>‡</sup> G. W. Mulholland,<sup>\*§</sup> and J. W. Gentry<sup>‡</sup>

Department of Chemical and Nuclear Engineering, University of Maryland, College Park, Maryland 20742, and National Bureau of Standards, Gaithersburg, Maryland 20899

Received August 12, 1986. In Final Form: December 15, 1986

The structure of soot agglomerates formed by the combustion of acetylene in a coannular diffusion burner is studied. Structural data from electron micrographs were obtained by two methods, particle counting with the aid of stereopairs for small clusters and electronic digitization with high-resolution image processing, used for the larger agglomerates. Langevin dynamics computer simulations based on free molecular motion were performed as an aid to interpreting the experimental results. Small agglomerates (with overall size  $<1.0 \mu\text{m}$ ) were found to have a fractal dimension of 1.5–1.6 compared to about 1.9 obtained by computer simulations. The power law exponent for the pair correlation function obtained over a limited range in  $r$  was found to be consistent with the value obtained by computer simulations for agglomerates in the 5–12- $\mu\text{m}$  range but somewhat greater for the agglomerates larger than 12  $\mu\text{m}$ . From the simulations it appears that the range of power law behavior for the pair correlation function based on the projected images is less than the range for the pair correlation function based on three-dimensional (3-D) structure.

## Introduction

The combustion of fossil fuels produces ultrafine soot particles evolved from a complex growth process involving nucleation, surface growth, and coagulation.<sup>1</sup> These particles may initially fuse upon collision. Eventually, however, the structural integrity of the particles is maintained, and clusters made up of these individual primary particles (approximately 20–30-nm diameter) are formed (see Figure 1). The structural analysis of these soot agglomerates is the subject of this paper.

The study of tenuous, low-density structures such as soot has become an active area of research. This is especially true in regard to the use of computers to simulate the growth of these structures. An important characteristic of many of these structures is a power law relationship between the mass, or number of particles  $N$ , and the radius of the cluster,  $R$ :

$$N = kR^{D_f} \quad (1)$$

The quantity  $D_f$  is the fractal or Hausdorff dimension.<sup>2</sup> While the value of  $D_f$  depends on certain features of the growth process, it has the general characteristic of always being less than the Euclidean dimension  $d$ . This implies that the average density of a fractal agglomerate decreases with increasing radius.

Experimental studies of actual agglomeration processes have shown similar mass-size relationships. Weitz and Huang<sup>3</sup> obtained a fractal dimension of about 1.70 for gold colloidal agglomerates based on electron microscopy and scattering measurements. Feder et al.<sup>4</sup> obtained a dimensionality of about 2.53 for protein aggregates. It is thought that the very low sticking probability is responsible for the more compact structure in this case. The inorganic "smokes" studied by Forrest and Witten,<sup>5</sup> including Fe, Zn, and SiO<sub>2</sub>, are expected to be formed by growth dynamics similar to that of soot, in contrast to other classes of aggregates. Forrest and Witten obtained fractal dimensions between 1.7 and 1.9 based on the size dependence of the pair correlation function obtained from TEM (transmission electron microscopy) images of the agglomerates.

Martin et al.<sup>6</sup> have also measured the fractal dimension of SiO<sub>2</sub> agglomerates produced in the vapor phase. The particles were from the same source as the SiO<sub>2</sub> agglomerates studied by Forrest and Witten. The analysis of Martin et al. was based on the intensity of scattered light as a function of the momentum transfer,  $q$ , for the particles dispersed in a liquid. The fractal dimension was found to be 1.84, in reasonable agreement with the value obtained by electron microscopy. With light scattering, the entire structure of the agglomerate is probed, while with electron microscopy only the 2-D projection is obtained. A disadvantage of light scattering is that the measurement is affected by the distribution of primary particle sizes and cluster sizes in addition to the fractal structure.

The extensive structural analysis of carbon black by Medalia and Heckman<sup>7,8</sup> was carried out before the development of fractal theory. The primary agglomerates of carbon black were characterized in terms of bulkiness, anisometry, and shape factors. The carbon black had been dispersed in a liquid by using ultrasonics prior to collection on electron microscope grids. The projected area of each agglomerate,  $A_r$ , was measured as a function of number of particles  $N$ . It was determined, for  $5 < N < 250$ , that

$$N = (A_r/A_p)^\alpha \quad \alpha = 1.1 \quad (2)$$

where  $\alpha$  is the projected area exponent and  $A_p$  is the average area of a primary particle in an agglomerate. One cannot quantitatively determine the fractal behavior on the basis of their results. For structures with a fractal dimension less than 2.0 (as suspected for soot agglomerates), little overlap in mass occurs upon projection, and

(1) Siegla, D. C.; Smith, G. W. *Particulate Carbon Formation During Combustion*; Plenum: New York, 1983.

(2) Mandelbrot, B. B. *The Fractal Geometry of Nature*; W. H. Freeman & Co.: New York, 1983.

(3) Weitz, D. A.; Huang, J. S. In *Kinetics of Aggregation and Gelation*; Family, F., Landau, D. P., Eds.; Elsevier Science: Amsterdam, 1984; p 19.

(4) Feder, J.; Jossang, T.; Rosenqvist, E. *Phys. Rev. Lett.* 1984, 53, 1403.

(5) Forrest, S. R.; Witten, T. A. *J. Phys. A* 1979, 12, n5, L109.

(6) Martin, J. E.; Schaefer, D. W.; Hurd, A. J. *J. Phys. A* 1986, 33, n5, 3540.

(7) Medalia, A. I.; Heckman, F. A. *J. Colloid Interface Sci.* 1967, 24, 393.

(8) Medalia, A. I.; Heckman, F. A. *J. Colloid Interface Sci.* 1971, 36, 173.

<sup>\*</sup>Presented at the symposium on "Fine Particles: High Temperature Synthesis", June 15–18, 1986, Atlanta, GA; G. Mulholland, Chairman.

<sup>†</sup>University of Maryland.

<sup>§</sup>National Bureau of Standards.

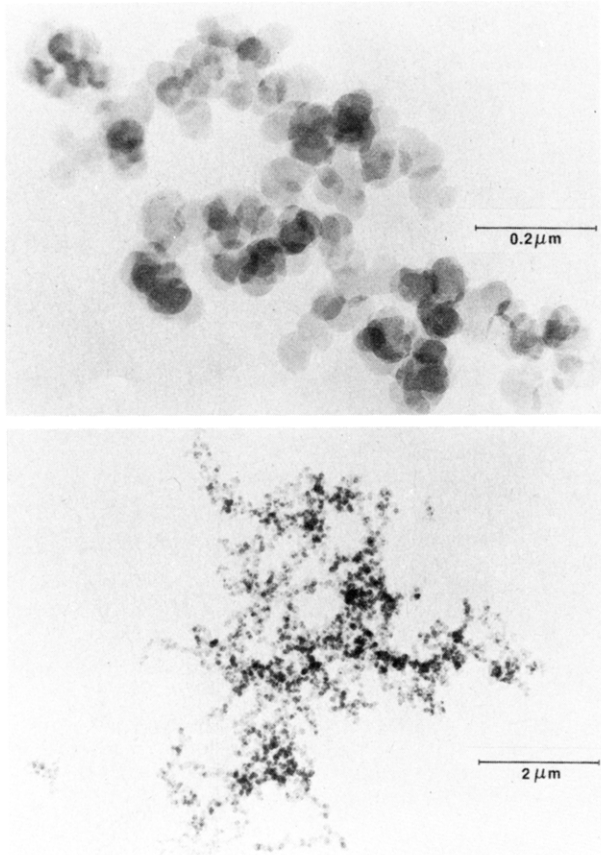


**Figure 1.** Samples of soot agglomerates formed by acetylene combustion.

the cluster is essentially transparent when viewed at any orientation. In the limit of large  $N$ , the fraction of particles evident upon projection becomes constant. As a result,  $N$  becomes proportional to  $A_r$ , and  $\alpha$  therefore has a limiting value of 1.0. Meakin<sup>9</sup> has verified that  $\alpha$  approaches 1.0 for large clusters on the basis of a computer simulation of cluster-cluster aggregation.

From X-ray and light scattering measurements, Schaefer et al.<sup>10</sup> determined carbon black agglomerates to be non-fractal or perhaps fractal ( $D_f = 2.1$ ) only over a limited regime. Unlike the soot examined in this study, the carbon black agglomerates were dispersed in water where a breakdown in agglomerate size can occur, resulting in smaller cluster sizes. Therefore, information on cluster size distribution becomes necessary.

The focus of this study is the structural analysis of both small and large agglomerates produced by a coannular diffusion burner, which has been extensively analyzed.<sup>11</sup> The use of an adjustable sample mount with the electron microscope allowed analysis of the agglomerate density distribution from several tilt angles and observation of the 3-D structure from viewing stereopairs. A significant element in this study is the use of computer simulations as a calibration check on the data analysis techniques. We obtain the pair correlation for the entire agglomerate, while other studies have focused on the internal portion of the agglomerate. The pair correlation function is needed for

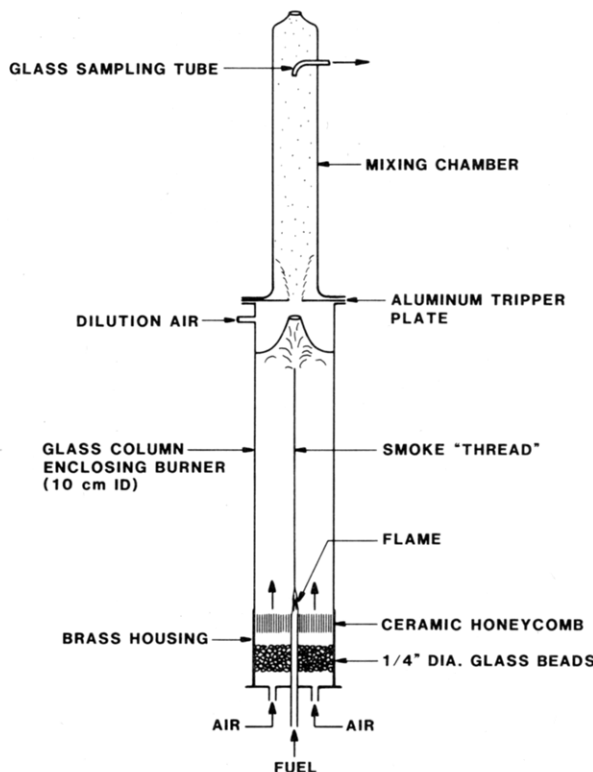


**Figure 2.** Schematic of coannular diffusion burner with mixing chamber.

describing the optical and hydrodynamical properties of the agglomerate.

One of the earliest models of cluster growth was developed by Sutherland and Goodarz-Nia,<sup>12</sup> in which flocculation occurred by random linear collisions of both particles and clusters. The simulation technique used in our study is based on a model which follows the Langevin trajectory of each agglomerate with the condition that particles stick upon collision.<sup>13</sup> To simulate the high-temperature, small particle size in the flame, the particle motion is treated as free molecular. The controlling parameter in the simulation is the relaxation time of the agglomerate,  $\beta^{-1}$ . The free molecular condition corresponds to  $\beta^{-1}$  being long compared to the time,  $\tau$ , to free stream a particle diameter. That is,

$$\beta\tau \ll 1 \quad (3)$$

In this paper we consider the case for  $\beta\tau = 0.05$ . This condition corresponds to the agglomerate moving approximately 20 primary particle diameters before changing direction. The random linear trajectory model corresponds to the limiting case for which  $\beta\tau = 0$ . The simulation is begun with 8000 particles in a box with a density  $0.0167/\sigma^3$  where  $\sigma$  is the primary particle diameter.

A second model used more as a qualitative tool in this study was the diffusion-limited aggregation (DLA) model introduced by Witten and Sander.<sup>14</sup> In this case a single particle diffuses via random walks on a lattice toward a stationary seed. The DLA aggregates appear dense and compact with a fractal dimensionality of 2.50. This is not expected to be a good model for soot growth, since all the clusters are diffusing. Only if the agglomeration occurred on the TEM grid as a result of addition of one primary particle at a time would this model be expected to be valid.

(9) Meakin, P. *J. Colloid Interface Sci.* 1984, 102, 491.

(10) Schaefer, D. W.; Martin, J. E.; Hurd, A. J. In *Physics of Finely Divided Matter*; Boccardo, N., Daoud, M., Eds.; Springer-Verlag: New York, 1985; p 31.

(11) Santoro, R. J.; Semerjian, H. G.; Dobbins, P. A. *Combust. Flame* 1983, 51, 203.

(12) Sutherland, D. N.; Goodarz-Nia, I. *Chem. Eng. Sci.* 1971, 26, 2071.

(13) Moutain, R. D.; Mulholland, G. W.; Baum, H. *J. Colloid Interface Sci.* 1986, 114, 67.

(14) Witten, T. A.; Sander, L. M. *Phys. Rev. Lett.* 1981, 47, 1400.

## Experimental Section

**A. Generation of Soot.** A coannular diffusion burner illustrated in Figure 2 was used to produce the soot agglomerates. The burner design is similar to that used by Santoro et al.<sup>11</sup> to obtain particle concentration profiles optically within the flame. Dobbins and Megaridis<sup>15</sup> have observed soot agglomerate structures within an ethene flame for the same burner by using a specially designed thermophoretic probe. Acetylene (99.9%) is chosen as the fuel source due to its high sooting tendency. The nominal fuel velocity is 0.8 cm/s. A tube length of 16 cm eliminates possible entrance effects for the 1.6-cm-i.d. tube and assures fully developed flow (length  $> 0.04 \times$  Reynolds number).

Air is introduced through two inlet ports at the bottom at a rate of 40 L/min and flows laminarly and uniformly across the top. Premixing of air and fuel is not allowed prior to combustion (diffusion flame). The air is dispersed uniformly inside the burner as it flows through a chamber packed with glass beads (0.64-cm diameter). Laminar flow is achieved by passage through a 2.54 cm thick ceramic honeycomb with 1.0 mm wide vertical channels. A glass chimney with a height of 53 cm (about 3 mm thick) encloses the entire burner from its base to a height of about 40 cm. This proved to be crucial in preventing external air currents caused by laboratory exhausts from distorting the steady flame and soot path. The stack was constructed of glass to allow the operator to visually monitor the flame and the sootting conditions.

Once the proper air and fuel flow rates are selected, the fuel is ignited, and a glass chimney is placed over the burner. A fine thread of smoke emerges from the laminar flame which extends to a height 30–35 cm from the base of the flame. At this height some backmixing occurs due to the flow constriction at the top, as evidenced by the dispersion of the fine thread of smoke in this area. Agglomeration begins in the flame and proceeds as the clusters traverse the length of the thread. At a fuel flow rate of 1.0 cm<sup>3</sup>/s, a very fine thread of smoke emerges from the flame and the overall agglomerate diameter ranges from 0.1 to 1.0  $\mu\text{m}$ . Most of the agglomeration in this case may be occurring in the flame itself. As the fuel flow is increased to 1.5 cm<sup>3</sup>/s, the laminar smoke thread becomes much darker as a larger fraction of soot produced in the flame breaks through the burnout region. Presumably intense growth in the smoke "thread" is responsible for agglomerates up to 50  $\mu\text{m}$  in overall diameter. The species are sampled by briefly passing TEM carbon-coated grids (3-mm diameter, 0.13 mm thick, and 200 mesh copper) over the top of the column with the mixing chamber and tripper plate removed. The agglomerates are primarily drawn toward the grids by thermophoresis.<sup>16</sup> Samples were collected only for a short period of time to avoid collection of clusters on top of one another on the TEM grid.

**B. Soot Characterization.** In order to provide an overall characterization of the soot generation process, size distribution and soot efficiency measurements were made in addition to the TEM analysis. To ensure a uniform soot concentration across the sampling area, the gas and particle mixture exiting the chimney is diluted with an additional 20 L/min of air and is dispersed by a tripper plate (2.54 cm; see Figure 2). A second stack (mixing chamber) placed directly on the plate allows turbulent mixing so that the soot concentration is uniform at the sampling point located 30 cm above the tripper plate.

Size distributions for two flow rates were determined by using an Anderson 2000 cascade impactor,<sup>17</sup> which has a fractionation range between 0.4 and 10- $\mu\text{m}$  aerodynamic diameters. The term "aerodynamic diameter" refers to a unit density sphere (density = 1.0 g/cm<sup>3</sup>) having the same settling velocity as the soot agglomerate. The average aerodynamic diameters at 0.7 and 1.2 cm<sup>3</sup>/s were found to be 0.48 to 5.8  $\mu\text{m}$ , respectively. The soot emission at 1.2 cm<sup>3</sup>/s acetylene flow rate was found to be 0.064 g of soot per g of C<sub>2</sub>H<sub>2</sub> burned.

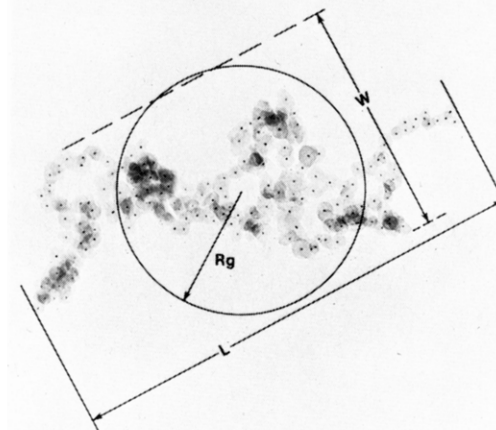


**Figure 3.** Digitized micrograph of a cluster consisting of 164 particles, illustrating agglomerate size parameters  $L$ ,  $W$ , and  $R_g$ . For this case,  $2R_g/d = 14.2$  and  $(LW)^{1/2}/d = 19.2$ , where  $d$  is the average primary particle diameter.

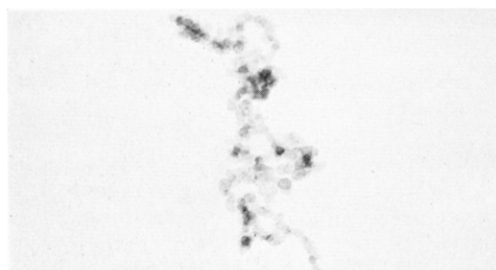


**Figure 4.** Stereopair of the agglomerate shown in Figure 3.

**C. TEM Image Processing.** The TEM images can be classified into two cluster size categories. The first category consisted of clusters with up to 200 primary particles, having overall diameters from 0.1 to 1.0  $\mu\text{m}$ . Magnifications in this category ranged from 73 to 330K $\times$ , depending upon cluster size and image resolution. In the particle counting method, the micrographs were enlarged to 20  $\times$  25 cm photographs, and the center of each primary particle was recorded on a Hewlett-Packard 87 with a digitizing tablet. Figure 3 is one such image. To aid in distinguishing overlapping particles, the agglomerates were examined in stereopairs, which consist of micrograph pairs of the soot viewed at two angles (about 10° apart). The JEOL 200CX transmission electron microscope has a viewing stage that is capable of tilting the TEM grid sample by 40° in either direction. Examining stereopairs through a stereoviewer enables one to recognize three-dimensional features of the agglomerate. An example of

(15) Dobbins, R. A.; Megaridis, C. M. *Langmuir*, in press.

(16) Davies, C. N. "Aerosol Science"; Academic: New York, 1966.

(17) Certain commercial equipment, instruments, and materials are identified in this paper to specify adequately the experimental procedure. In no case does such identification imply recommendation or endorsement by the National Bureau of Standards or University of Maryland, nor does it imply that the material or equipment identified is necessarily the best available for the purpose.

a stereopair is shown in Figure 4. Gray et al.<sup>18</sup> observed a 36% increase in the number of particles for diesel soot agglomerates by use of stereopairs compared to conventional viewing of 2-D images.

Agglomerates between 5 and 40  $\mu\text{m}$  constitute the second size category. In this set, each micrograph is converted to an electronic grid of  $512 \times 512$  pixels. Each pixel, as viewed on a high-resolution monitor, has an associated gray level which can have values from 0 to 255. A gray level of 0 signifies the darkest gray, while 255 the highest gray level. By use of a Lisp-based image analysis system developed by Bright,<sup>19</sup> appropriate gray level "thresholds" are chosen to determine which pixels represent areas on the grid that are occupied by a particle. For example, if a digitized image is assigned a value of 155, all pixels with levels from 155 to 255 are reset to 255 (white), while pixel gray levels from 0 and 154 are set to 0 (black). Note that the micrographs are negatives with clusters light gray against a dark background. The end result is a  $512 \times 512$  array representing the threshold version of the digitized image. For simplicity, values of 255 are set to 1.0 so the array consists of only 1's and 0's. Array values of 1.0 are termed "occupied sites" since they signify the presence of a particle, in either a portion or its entirety, at that location. Surrounding clusters not associated with the cluster of interest are eliminated from the threshold version by assigning corresponding pixels a value of 0.0. Data in this category are evaluated by the successive square, pair correlation, and Sullivan<sup>20</sup> methods.

### Data Analysis

In this section, the techniques used to determine  $D_f$  will be discussed in greater detail. We noted in the previous section that all the data pertaining to  $D_f$  were obtained from TEM micrographs of agglomerates. Consequently, it is our goal to obtain 3-D structural information from the 2-D TEM images. The data analysis procedures to be discussed later in this section depend on the assumption that essentially all particles are evident upon projection, i.e., that the agglomerate is transparent and only a few particles are completely masked by others. The validity of this assumption depends on the fractal dimension being less than 2.0, which is believed to be the case for these agglomerates. Mandelbrot<sup>21</sup> states that  $D_f < 2.0$  implies that the projection typically itself is of dimension  $D_f$ . Weitz and Huang<sup>3</sup> offer a simple argument based on the relation

$$M \sim R^{D_f} \quad (4)$$

which is the same form as eq 1 with  $N$  replaced by the cluster mass  $M$ . Since the 3-D fractal ( $D_f < 2.0$ ) is transparent,  $M$  determined from the two-dimensional projection will be equivalent to the total mass of the object in three dimensions. Also,  $R$  obtained from the projection will be essentially the same as the value determined from the three-dimensional structure. Thus the projection is a fractal with the same  $D_f$  as the three-dimensional shape. We shall further discuss the validity of this statement in light of the analysis of simulation clusters in 3-D and their projections.

**A. Particle Counting Method.** In this method, the total number of primary particles are determined as a function of cluster size. The clusters chosen are limited to those consisting of 200 particles or less, beyond which one encounters increasing difficulty in distinguishing overlapping and partially fused spheres, even with stereopairs. Two definitions of cluster size are used (see Figure

Table I. Typical Results for the Particle Counting Method

$N$	$\bar{d}$ , nm	$\sigma$ , nm <sup>a</sup>	$R_g/\bar{d}$	$(LW)^{1/2}/\bar{d}$	$L/W^b$
5	27.9	2.0	.55	2.33	1.15
10	30.9	4.1	1.56	3.93	1.91
13	28.7	2.9	1.19	4.46	1.29
14	28.5	3.5	1.18	4.24	1.33
21	25.5	2.0	1.85	5.96	1.39
22	21.1	2.0	1.41	4.97	1.24
23	34.2	2.3	2.12	5.57	1.72
31	26.2	3.5	2.05	6.53	1.02
39	22.0	1.7	2.27	6.33	1.88
46	27.3	2.7	3.11	8.68	1.58
52	23.8	2.9	2.87	9.30	1.08
56	29.3	2.0	2.98	9.57	1.08
57	26.4	2.4	3.21	9.06	1.88
68	30.6	3.0	4.22	12.7	1.33
82	22.1	3.0	4.82	12.4	1.74
99	35.8	2.7	4.62	13.1	1.68
107	41.6	8.8	5.25	14.0	1.50
109	31.4	3.9	6.24	14.3	2.79
162	34.8	9.3	7.45	22.4	1.21
164	28.1	3.9	7.12	19.2	2.06

<sup>a</sup>  $\sigma$  refers to the standard deviation of mean  $d$ . <sup>b</sup> Average  $L/W$  for entire set is 1.68,  $\sigma = 0.50$ .

3): the first is in terms of the geometric mean of the cluster length,  $L$ , and  $W$ , the projected length perpendicular to the axis through  $L$ , and the second definition is in terms of the radius of gyration  $R_g$ , as given by

$$m_T R_g^2 = \sum_{i=1}^N (m_i r_i^2) \quad (5)$$

where  $m_T$  is the total mass of the cluster and  $m_i$  is the mass of particle  $i$  whose center is at a distance  $r_i$  from the centroid. Since, the primary particle size varied from cluster to cluster (see Table I),  $R_g$  was normalized by dividing its value by the average particle diameter  $\bar{d}$  for the cluster. Values of  $\bar{d}$  were obtained by arbitrarily choosing 10 representative primary particles from each cluster. The geometric mean  $(LW)^{1/2}$  was normalized in the same fashion as  $R_g$ . A useful quantity is the ratio  $L/W$ , which provides a description of overall cluster shape. To test whether the cluster growth is fractal, we plotted  $\log N$  vs.  $\log (size)$ . For fractals a linear dependence with a slope of  $D_f$  will be observed (eq 1). We follow Meakin's<sup>9</sup> notation by referring to the exponent determined in this manner as  $D_\beta$ .

**B. Analysis of Large Clusters (5–40  $\mu\text{m}$ ).** 1. Successive Squares Method. As previously mentioned, the digitized data from electron micrographs of large clusters consisted of  $512 \times 512$  arrays with values of 1's (occupied site) or 0's (unoccupied site). The first method to evaluate  $D_f$  from this data set involved placing series of nonoverlapping squares of side  $l$  from the center of mass of the agglomerate. The total number of sites occupied within each square is then determined as a function of  $l$ . This is similar to the nested square method of Forrest and Witten,<sup>5</sup> except that the center of all the squares are the same in our analysis. In the nested squares method, the square center location was chosen as the point where the center of mass of occupied sites within the square and the geometric center of the square coincided. For a fractal,  $N$  will vary as  $l^{D_f}$ . A weighted fit of  $\log N$  vs.  $\log l$  was performed, assuming that the square of the probable error for each point varied as  $N^{-1/2}$ .

**2. The Pair Correlation Method.** The pair correlation function  $c(r)$  is the average density of occupied points in the digital image at a distance of  $r$  from each occupied point:

$$c(r) = 1/(2\pi r N) \sum (\rho(\mathbf{r} + \mathbf{r}')\rho(\mathbf{r}')) \quad (6)$$

(18) Gray, R. H.; Kanapilly, G. M.; Cheng, Y. S.; Wolff, R. K. J. *Aerosol Sci.*, 1985, 16, 211.

(19) Bright, D. S., submitted for publication in *J. Microsc.*

(20) Hunt, F.; Sullivan, F. In *Dimensions and Entropies in Chaotic Systems*; Mayer-Kress, G., Ed.; Springer-Verlag: New York, 1986; p 74.

(21) Mandelbrot, B. B. "Fractals—Form, Chance, and Dimension"; W.H. Freeman: and Co.: New York, 1977.

where  $N$  is the total number of occupied sites,  $\rho(\mathbf{r}')$  the density at a reference point vector  $\mathbf{r}'$ ,  $\rho(\mathbf{r} + \mathbf{r}')$  the density at vector  $\mathbf{r} + \mathbf{r}'$ , equal to 1.0 if occupied and 0 otherwise, and the summation is over all sites. The notation  $\langle \dots \rangle$  represents orientational averaging. The pair correlation function for a fractal structure would have the following dependence on  $r$

$$c(r) \sim r^{D_f - d} \quad (7)$$

where  $d$  is the Euclidean dimension.<sup>22</sup>

The use of a  $512 \times 512$  lattice, however, places a limit on the number of points (occupied or unoccupied) that are a distance of  $r$  around each point. Consequently, we approximate this density as the density of occupied sites in a shell of inner radius  $r - 0.5$  and outer radius  $r + 0.5$ . This density is computed for every occupied site and the average of these densities for a fixed distance  $r$  is defined as  $c(r)$ . This is done for a reasonable range of  $r$  values (1–200-pixel spacings). For a fractal,  $c(r)$  would vary as  $r^{D_f - d}$ , where  $d = 2$ . In practice this form is expected to be valid for  $r$  large compared to the size of a primary particle and small compared to the overall size of the agglomerate. Again, following Meakin's notation, we use the symbol  $D_a$  to refer to the power law obtained by the pair correlation method.

A computer program is used to compute  $c(r)$ . In the program, the distances between every particle, rounded off to the nearest integer, is determined. Then the number of occurrences of each distance is recorded in array  $n(i)$ . If  $n(51) = 2100$ , for example, the total number of times when an occupied site is at a distance of  $r \approx 51$  to another occupied site is 2100. The value of  $c(r)$  is computed by dividing  $n(i)$  by the total number of occupied sites  $N$  and by the total number of points (occupied and unoccupied) in a shell of inner radius  $r - 0.5$  and outer radius  $r + 0.5$  in a square lattice.

**3. The Covering Set Approach.** The third method used for the  $512 \times 512$  data set is a program developed by Hunt and Sullivan.<sup>20</sup> Given a set of points in space, the following relationship holds true if the set is a fractal:

$$K(a) = a^{-D_f} \quad (8)$$

where  $K(a)$  is the number of segments (in one dimension) of length  $a$  needed to cover the set. Similarly,  $K(a)$  for a two- or three-dimensional set would correspond to the number of circles or spheres of radius  $a$ . This method determines  $K(a)$  for  $a$  given in factors of  $1/2$  (i.e.,  $1/2, 1/4, \dots$ ). The points belonging to the  $512 \times 512$  array are scaled between 0 and 1 prior to analysis. This approach provides for an efficient "tree" algorithm that has a short execution time since  $K(a)$  is evaluated at values of uniform distribution in a log-log plot and because the code is suitable for vector programming on the Control Data Corporation Cyber 205 supercomputer.

The pair correlation and Sullivan's method were verified using a two-dimensional fractal known as a Sierpinski carpet with a fractal dimension  $D_f \approx 1.89$ , along with compact ordinary objects with  $d = 2$ . The dimensions computed were within 2% of the true values. In the next section, the experimental values of  $D_f$  for the soot agglomerates, along with other structural features, are presented. These results are then compared with simulations and past experimental studies of inorganic smokes.

## Experimental Results

**A. Particle Counting Method.** Thirty-seven clusters were collected and evaluated by the particle counting

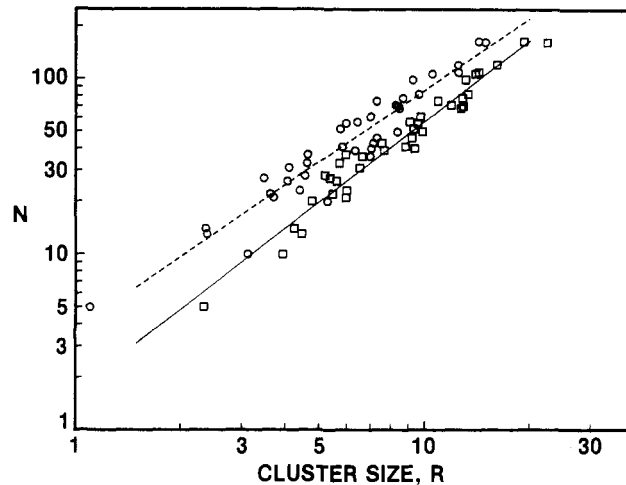


Figure 5. Number of particles,  $N$ , vs. size,  $R$ , for experimental data. Cluster sizes defined as  $2R_g$  ( $\circ$ ) and  $(LW)^{1/2}$  ( $\square$ ).

method. Table I is a listing of cluster size as a function of  $N$  for a few of the samples collected. Our own ability to distinguish individual particles limited the size range to  $5 \leq N < 200$ . The results are summarized in Figure 5. The linearity observed indicates a mass-size power law relationship described by eq 1. Fractal dimensions of  $1.61 \pm 0.13$  and  $1.49 \pm 0.16$  for cluster sizes defined by  $(LW)^{1/2}$  and  $R_g$ , respectively, were obtained by linear regression. The aspect ratio  $(L/W)$  of the agglomerates varied from about 1.0 (nearly spherical) to about 2.0 (elongated structure). The average agglomerate length to width ratio was 1.68 ( $\sigma = 0.50$ ). No correlation was observed between the aspect ratio and the number of spheres in the agglomerate.

Since the possibility of undercounting is greater for large agglomerates due to the overlap of particles, the slope of both experimental lines should be slightly lower than the true fractal dimension. As seen in Figure 3, there are certain regions of high overlap where undercounting is likely. Below we show how undercounting of  $N$  may further reduce the value of  $D_f$  when using  $R_g$  as cluster size.

We let  $n$  represent the difference between the actual number of spheres,  $N$ , and the measured number,  $N_m$ . Expressing eq 5 in terms of  $N$ ,  $N_m$ , and  $n$ , we obtain

$$NR_g^2 = N_m R_{gm}^2 + \sum_{i=1}^n r_i^2 \quad (9)$$

where  $R_{gm}$  is the measured radius of gyration and  $r_i$  now represents the distance from the center of mass to the  $i$ th sphere ( $i = 1-n$ ) not accounted for in the measurement. Rearranging eq 9, we obtain

$$R_g/R_{gm} = \frac{[N_m + \sum_{i=1}^n r_i^2/R_{gm}^2]^{1/2}}{(N_m + n)} \quad (10)$$

A two-term Taylor series expansion is performed to obtain the final expression:

$$R_g/R_{gm} \approx 1 + (1/2) \frac{[\sum_{i=1}^n r_i^2/R_{gm}^2 - n]}{(N_m + n)} \quad (11)$$

In general, overlaps are present near the agglomerate center of mass. Now consider a situation where 20% undercounting has occurred, i.e.,  $N_m = 0.8N$  and  $n = 0.2N$ .

Table II. Structural Data and Calculated Values of the Fractal Dimension  $D_f$ 

image no.	magnification, KX	$D_f$		no. of occupied sites	range of $r$ in $c(r)$	$(LW)^{1/2}$ , $\mu\text{m}$	$L/W^a$	nm/pixel (approx.)
		$c(r)$	Sullivan					
2313-115 <sup>b</sup>	10	1.82 ± 0.02	1.82	1.86	39 708	2-23	7.0	1.1
2313-120		1.81 ± 0.02	1.81	1.88	37 751	2-26		
2313-125		1.80 ± 0.02	1.80	1.83	35 804	2-24		
2315	10	1.81 ± 0.02	1.81	1.87	30 067	2-25	5.5	1.6
2500	7.3	1.80 ± 0.05	1.77		25 453	2-11	7.3	1.5
2509	6	1.86 ± 0.02	1.84	1.94	33 620	2-20	9.1	3.0
2510	5	1.81 ± 0.01	1.83		39 489	2-37	12.0	1.1
2507	5	1.93 ± 0.01	1.87	1.95	72 890	2-23	13.8	1.3
2504	2	1.85 ± 0.02	1.83	1.79	29 916	2-22	22.0	1.8
2505	2	1.91 ± 0.01	1.85	1.95	49 266	2-30	24.6	1.9
2506	2	1.92 ± 0.01	1.87	1.92	63 472	2-24	36.1	1.2
2516-0°	2	1.94 ± 0.01	1.88	1.95	72 358	2-21	35.5	1.1
2516-45°		1.94 ± 0.01	1.90	1.95	69 776	2-22	30.0	1.4
2512	1.5	1.90 ± 0.01	1.83	1.83	27 858	2-17	33.2	2.5
2515	1.5	1.90 ± 0.01	1.81	1.66	29 303	2-16	29.2	2.1
2513	1.5	1.84 ± 0.06	1.76	1.82	19 701	2-7	38.0	2.9
test images								
Sierpinski								
Carpet		1.86 ± 0.02	1.90		32 768	2-10		1.0
square		1.98 ± 0.01	2.00	2.00	155 236	1-18		1.0
rectangle		1.99 ± 0.01	2.00	2.00	154 184	1-15		3.0

<sup>a</sup>Mean  $L/W = 1.8$ ,  $\sigma = 0.66$ . <sup>b</sup>115, 120, and 125 are gray level thresholds.

For the extreme case of  $r_i = 0$  (overlaps at the center of mass), we get, from eq 11,

$$R_{gm} \approx 1.11R_g \quad (12)$$

and for  $r_i \approx 0.5R_g$ ,

$$R_{gm} \approx 1.08R_g \quad (13)$$

Equations 12 and 13 show that undercounting yields superficially higher  $R_{gm}$  values for large clusters resulting in too low a value for  $D_f$  by about 5%. This prediction is consistent with the experimental result (Figure 5) that  $D_f$  computed using  $R_g$  is smaller than the value computed from  $(LW)^{1/2}$ .

**B. Pair Correlation, Sullivan, and Successive Squares Methods.** In Table II, the results of the pair correlation, Sullivan, and successive squares methods are listed for the size range 5.5–38  $\mu\text{m}$ . Agglomerates quite similar in shape to those of the particle counting method were collected (i.e., elongated and spherical) but on a much larger scale. The average length to width ratio of these agglomerates was 1.8 ( $\sigma = 0.66$ ). The agglomerates have fractal dimensions between 1.75 and 1.95; however, in some cases the power law behavior of  $c(r)$  is observed over a very limited range.

The range of  $r$  where eq 7 is valid appears to be strongly dependent on the shape ( $L/W$ ). The quantity  $r$  is in units of pixels. Figure 6A,B is an example of clusters with high sphericity ( $L/W = 1.1$  and 1.2) where the power law is observed over a long range of  $r$  (2-37 and 2-24). On the other hand, cluster number 2513 ( $L/W = 2.9$ ) shown in Figure 6C is at best linear for the range  $r = 2-7$ . This is probably due to the fact that for elongated structures a greater percentage of the area around the edges is encountered as opposed to rounded ones. These areas of zero density significantly lower  $c(r)$  as seen in all cases as  $r$  approaches the size of the agglomerate. By the same token, smaller agglomerates ( $< 5 \mu\text{m}$ ) such as cluster number 2500 shown in Figure 6D, whose internal structures are not yet fully developed also display shorter power law ranges. A summary of the effects of cluster size and shape is illustrated in Figure 7, a combined plot of  $c(r)$  vs.  $r$  for  $r = 1-250$ . Agglomerates with  $L/W \approx 1$  are shown to have longer power law dependence over as much as two thirds

Table III. Resolution of Mass in Digitization Process

TEM magnification	no. of pixel lengths equaling one particle diam (30 nm)	TEM magnification	no. of pixel lengths equaling one particle diam (30 nm)
10K×	2.1	5K×	1.0
7.3K×	1.6	2K×	0.4
6K×	1.3	1.5K×	0.3

of the total range in log  $r$ . For elongated or underdeveloped structures, the quantity  $c(r)$  may have a power law behavior over only one-third of the range in log  $r$ .

As a test case,  $c(r)$  was determined for a solid square ( $L/W = 1.0$ ) and rectangle ( $L/W = 3.0$ ) of equal overall area with pixel length sizes comparable to that of the digitized soot agglomerate image. The result is plotted in Figure 8. For slopes equal to  $1.98 \pm .01$ , only a slightly longer range of linearity is found for the square (51% vs. 49% of total range in log  $r$ ). It is apparent that increasing aspect ratios does not fully explain the observed reduction of the power law range for the soot agglomerates. It is also of interest that even in this case the power law behavior of the pair correlation function is valid only over half the range in log  $r$ .

There is good agreement between the pair correlation and Sullivan approach for clusters between 5 and 12  $\mu\text{m}$ , corresponding to magnifications between 5K× and 10K×, respectively. Below 5K×, however,  $D_f$  values computed by the pair correlation approach are consistently higher (by  $\approx 0.10$ ) than those of greater magnification. For these clusters the determination of  $D_f$  from projected images may have a large uncertainty since  $D_f$  is approaching 2.0. It appears that the digitized images become denser for agglomerates larger than about 12  $\mu\text{m}$ , most of which are photographed at magnifications less than 5K×. We first consider the possibility that this increase in  $D_f$  for agglomerates of sizes  $\geq 12 \mu\text{m}$  is the result of instrument limitations or events unrelated to the growth phenomena. Specifically, there is an inherent decrease in resolution on a 512 × 512 lattice as more than one particle begins to occupy each pixel. Table III shows the approximate length between pixels in comparison with the average particle diameter at different magnifications. At a magnification of about 5K×, the length of one side of an occupied site

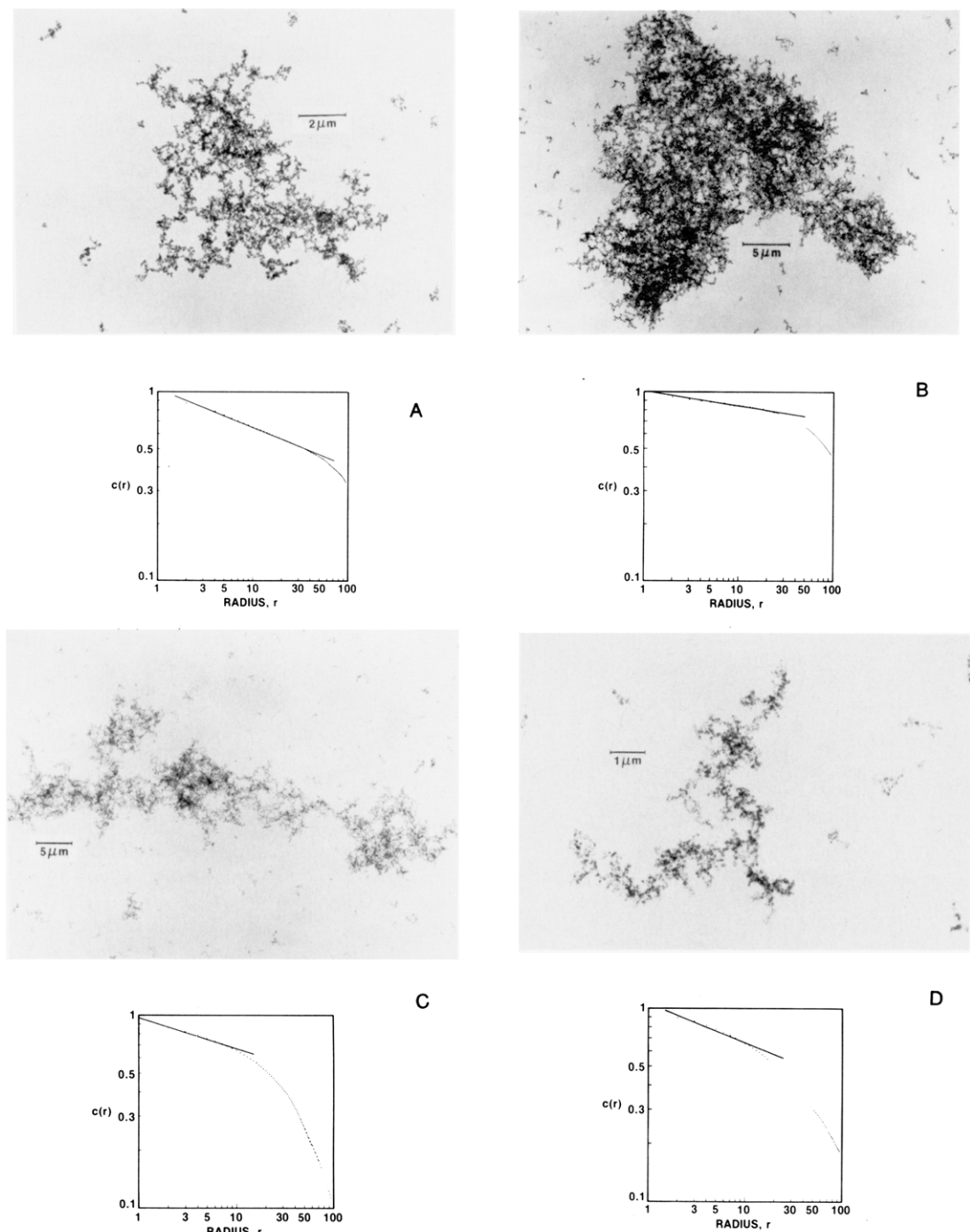


**Figure 6.** Micrograph and associated pair correlation,  $c(r)$ , plot where  $r$  is in pixel spacings, for a variety of agglomerate shapes: (a) Cluster no. 2510,  $L/W = 1.1$ ,  $(L/W)^{1/2} = 12.0 \mu\text{m}$ , fit  $r$  in the range 2–37. (b) Cluster no. 2506,  $L/W = 1.2$ ,  $(L/W)^{1/2} = 36.1 \mu\text{m}$ , fit  $r$  in the range 2–24. (c) Cluster no. 2513,  $L/W = 2.9$ ,  $(L/W)^{1/2} = 38.0 \mu\text{m}$ , fit  $r$  in range 2–14. (d) Cluster no. 2500,  $L/W = 1.5$ ,  $(L/W)^{1/2} = 7.3 \mu\text{m}$ , fit  $r$  in range 2–7.

is about equal to a particle diameter. The resolution further diminishes with decreasing magnification until at  $1.5K\times$  the length of one pixel corresponds to three particle diameters.

To measure the effects of decreasing resolution accurately, the  $512 \times 512$  array representing cluster number 2313 was reduced to a  $256 \times 256$  array of 1's and 0's. This was done by checking groups of  $2 \times 2$  pixels in the  $512 \times 512$  array for  $\geq 50\%$  occupancy (values of 1's). If  $\geq 50\%$  occupied, the corresponding location in the  $256 \times 256$  matrix is set to 1.0, otherwise it is 0. In effect, a  $256 \times 256$  matrix is obtained just as if the micrograph was digitized with such a resolution. The procedure is repeated to obtain a  $128 \times 128$  and  $64 \times 64$  matrix. The data were then

evaluated by the  $c(r)$  method. As shown in Figure 9, the power law slope is essentially the same for all four curves. Although deviations from power law behavior appear at different  $r$  values, these would actually correspond to approximately the same lengths if plotted vs. micrometers. We therefore conclude that the effect of low resolution does not result in a superficially higher  $D_f$  as suggested. In retrospect, if the agglomerates are indeed fractals, the internal structure is statistically scale invariant and changes in length scales (varying resolution) would not affect  $D_f$ . Whether bigger clusters result in larger exponents, which implies that some other physical mechanism takes over, will be discussed in the next section in light of computer simulations of cluster-cluster agglomeration.

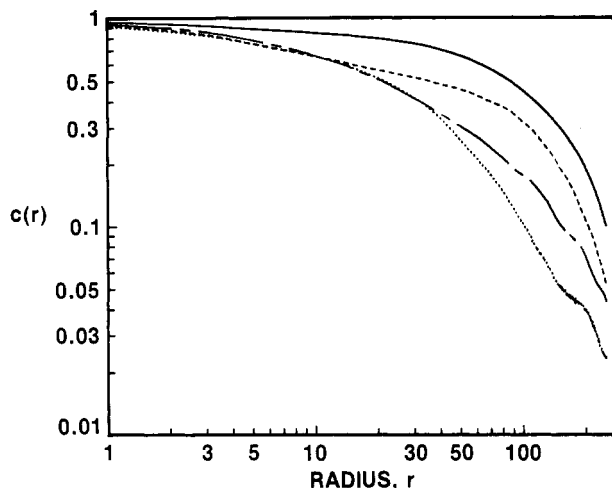


**Figure 7.** Comparison of pair correlation,  $c(r)$  plots for agglomerates in previous figures: (—) 2506, 2.0K $\times$ ,  $L/W = 1.2$ ; (---) 2510, 5.0K $\times$ ,  $L/W = 1.1$ ; (- -) 2500, 7.3K $\times$ ,  $L/W = 1.5$ ; (....) 2513, 1.5K $\times$ ,  $L/W = 2.9$ .

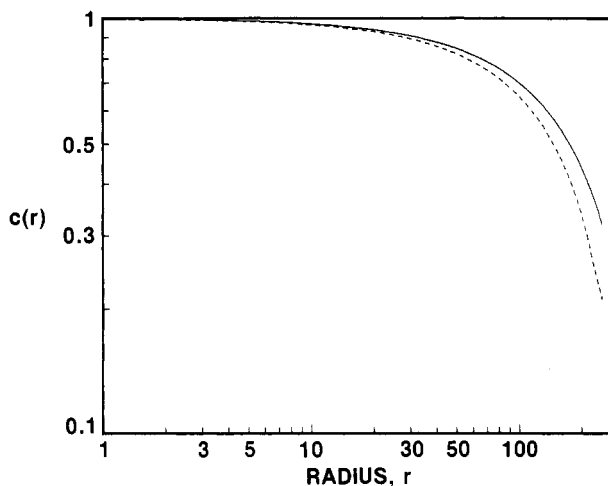


**Figure 8.** Pair correlation plots for test cases: (—) filled square,  $L/W = 1$ ,  $D_\alpha = 1.98 \pm 0.01$  for  $1 \leq r \leq 18$ ; (---) filled rectangle,  $L/W = 3$ ,  $D_\alpha = 1.98 \pm 0.01$  for  $1 \leq r \leq 15$ .

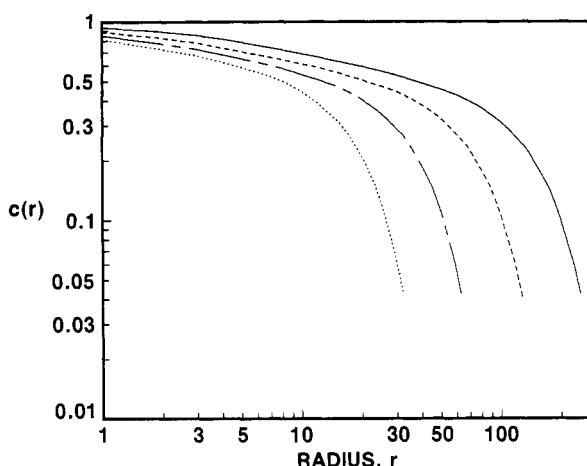


**Figure 9.** Effect of digitizer resolution on  $c(r)$ . Fractal dimension  $D_\alpha \approx 1.80 \pm 0.02$  in all cases: (—)  $512 \times 512$ ; (---)  $256 \times 256$ ; (- -)  $128 \times 128$ ; (....)  $64 \times 64$ .

To examine the possible effects of the imaging process on  $D_f$ , variations in threshold levels and tilt angles were investigated. Micrograph number 2313 was processed at threshold gray or brightness levels of 120, 125, and 130, and only a 1% change in  $D_f$  was found by the pair corre-

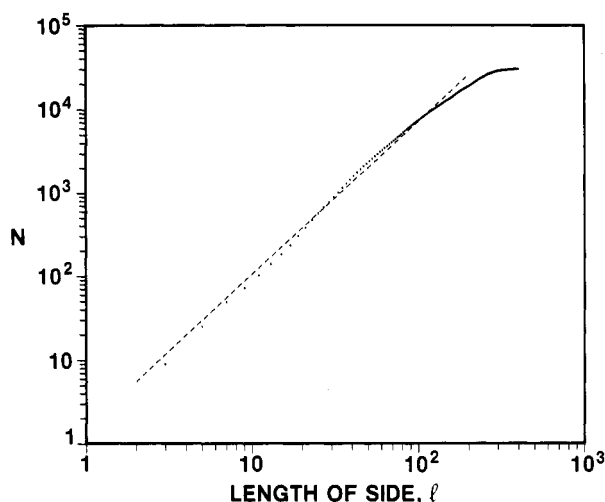


**Figure 10.** Successive squares method plot for cluster 2313;  $r$  in pixel spacings. Fit for  $l = 2-181$ ; slope  $D_f = 1.82$ .

lation and Sullivan methods. In general, a threshold value within  $\pm 5$  gray levels of those that represent a contiguous image resembling a silhouette of the agglomerate is chosen. In terms of the tilt angle, no significant effect was found. Cluster number 2313 was tilted through  $55^\circ$  and is represented by cluster 2315. As an aside, one can infer that the agglomerate extends out in all three directions as opposed to two. If growth proceeded along a plane, one would expect a dramatic increase or decrease in size as the sample is rotated, which is not the case for clusters 2313 and 2516 upon rotation. This also supports the assumption that the sample is not distorted or flattened on the TEM grid. These results indicate a moderate insensitivity toward thresholds and tilt angles. Consequently, the analyst has greater flexibility and control in the digitization process.

Generally higher values of  $D_f$  resulted from the successive squares method. Figure 10 is a plot of  $\log N$  vs.  $\log l$  with a slope of  $D_f = 1.83$ . This method, however, was found to be ineffective for clusters where the center of mass is in a region of unoccupied sites, characteristic of small agglomerates with few branches, resulting in nonlinearity. In regard to computer execution times, Sullivan's approach was found to be at least 2 orders of magnitude faster than the  $c(r)$  method.

### Discussion of Results

As stated earlier, two computer models were examined. The first is the diffusion-limited aggregation (DLA) model introduced by Witten and Sander<sup>14</sup> which allows single-particle diffusion via random walks toward a stationary seed. The second model (cluster-cluster agglomeration) applies the Langevin equation to particles and clusters undergoing Brownian motion in a nonlattice cube subject to periodic boundary conditions.<sup>13</sup> It is expected that the free molecular growth mechanism used in the simulation is most valid for the small clusters formed in the flame. Figure 11 shows comparative sizes of clusters obtained experimentally and those generated by DLA and cluster-cluster agglomeration. Note the similarities between the open and chainlike structures of experimental and cluster-cluster agglomerates. DLA aggregates appear more dense and compact, characteristic of its high dimensionality of 2.50. On the basis of appearance alone, it is obvious that cluster-cluster agglomeration best represents the soot agglomeration process.

For a quantitative comparison, we applied the fractal methods of analysis to the simulation clusters. We first

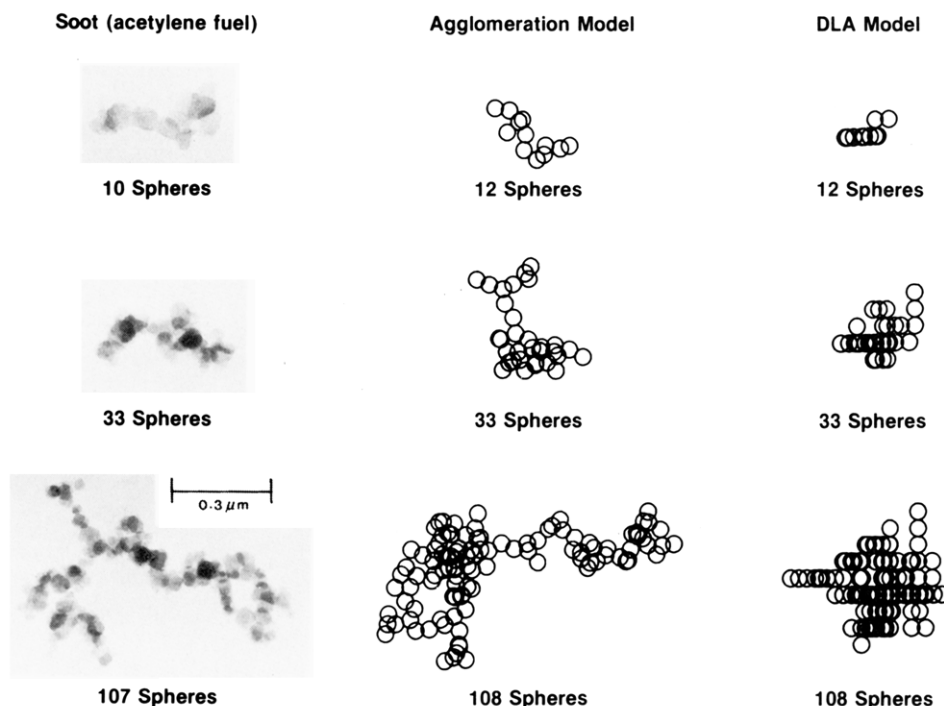


**Figure 11.** Qualitative comparison of clusters produced experimentally and by computer simulations for cluster-cluster agglomeration and diffusion-limited aggregation.

address the question of whether  $D_f$  is indeed invariant upon projection by applying the particle counting and pair correlation methods to clusters generated from the simulation of Mountain et al.<sup>13</sup> To provide a fair comparison with the experiment, the power law fit of  $N$  vs.  $R_g$  was based on a uniform selection of  $N$  on a log scale rather than linear scale, similar to the experimental distribution. The value of  $R_g$  for the projected image is computed for a single projection for each agglomerate. The value of  $N$  is the same for the projection as for the 3-D structure. For the particle counting method, the difference in the values of  $D_\beta$  ( $1.96 \pm 0.09$  in 3-D and  $2.00 \pm 0.12$  for projections) is within the uncertainty of the computation. The result of our simulation,  $D_\beta = 1.96$ , for agglomerates from 5 to 200 is to be compared to 1.85 obtained by Sutherland and Goodarz-Nia<sup>12</sup> for agglomerates from 4 to 256 and 1.81 obtained by Meakin<sup>9</sup> for clusters from 5 to 500. The latter two simulations are based on random linear trajectories. While there is minimal difference between the models, the experimentally determined  $D_\beta$  is significantly less than the simulations, even with the large experimental uncertainty as shown in Figure 12 ( $1.49 \pm 0.16$  based on  $R_g$  and  $1.61 \pm 0.13$  based on  $(LW)^{1/2}$  compared to about 1.90 for the models). The free molecular condition should be most valid for the growth of relatively small agglomerates in the flame. Other processes including particle charging and partial oxidation may affect the agglomerate structure in the flame.

To test the pair correlation approach, “digitized” projected images of the simulation agglomerates were numerically constructed. The pair correlation function for the projected image was determined by the same method as for the actual soot agglomerate. The fractal dimension based on the projected coordinates is about 0.15 less than the value based on the 3-D coordinates of the agglomerate (see Table IV). Meakin computed  $D_\alpha$  for the projections of 3-D agglomerates based on cluster-cluster aggregation with a size-independent diffusion coefficient. From the initial slope of  $\log c(r)$  vs.  $\log r$ , Meakin obtained  $D_\beta \approx 1.75$  for the projected agglomerate for two cluster sizes. For

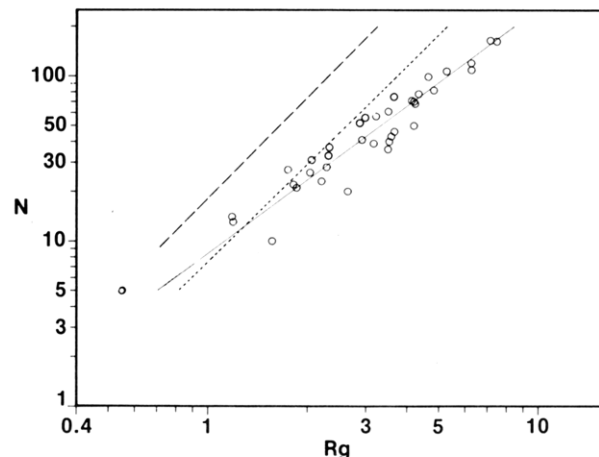


**Figure 12.**  $N$  vs.  $R_g$  plots of experimental and projected simulation data: (—) experimental; (---) diffusion-limited aggregation; (- - -) Langevin trajectory simulation.

**Table IV. Comparison of 3-D and Projected Values of  $D_f$  from Cluster-Cluster Simulation<sup>a</sup>**

$N^b$	$D_f$		
	3-D	projected 3-D	$L/W$
$\leq 5, \leq 200^a$	$1.96 \pm 0.09$	$2.00 \pm 0.12$	
932 <sup>c</sup>	$1.99 \pm 0.21$	$1.77 \pm 0.01^d$	1.03
1184 <sup>c</sup>	$1.74 \pm 0.20$	$1.77 \pm 0.02^d$	1.67
1052 <sup>c</sup>	$2.01 \pm 0.19$	$1.74 \pm 0.03^d$	1.85
1590 <sup>c</sup>	$1.74 \pm 0.15$	$1.72 \pm 0.05^d$	2.65
2841 <sup>c</sup>	$2.04 \pm 0.11$	$1.86 \pm 0.01^d$	1.51
1070 <sup>c</sup>	$1.94 \pm 0.13$	$1.75 \pm 0.04^d$	1.40
1593 <sup>c</sup>	$1.86 \pm 0.11$	$1.70 \pm 0.01^d$	1.31
mean	$1.90 \pm 0.13$	$1.76 \pm 0.05^d$	1.63

<sup>a</sup>  $\beta_r = 0.05$ ,  $\rho = 0.167$ ;  $\tau$  is the time required to free stream a particle diameter, set equal to 1.0. <sup>b</sup> Particle counting. <sup>c</sup> Pair correlation. <sup>d</sup> Numerically digitized projection.

the corresponding 3-D agglomerates, Meakin obtained values of 1.76 (2500 particle cluster) and 1.83 (5000 particle cluster) from the slope computed over the range  $r = 3-30$ .

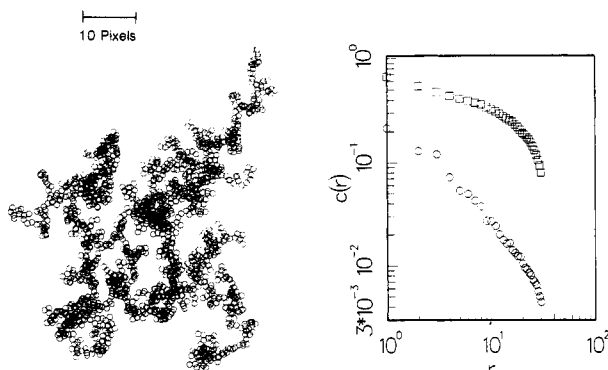


**Figure 13.** (Left)  $xy$  projection of computer-generated agglomerate with 1593 particles. (Right) 3-D pair correlation function ( $\circ$ ) and 2-D pair correlation function plot of numerically digitized projection ( $\square$ ) for agglomerate shown: slope of 3-D  $c(r)$  power law = 1.14,  $D_\alpha = 3.0 - 1.14 = 1.86$ ; slope of 2-D  $c(r)$  power law = 0.30,  $D_\alpha = 2.0 - 0.30 = 1.70$ .

The larger difference obtained based on the Langevin trajectory method may be a result of the higher initial concentration (0.0167 vs. 0.0025 and 0.005) and the smaller number of particles. The actual soot agglomerates have more than 5000 particles and are produced at concentrations orders of magnitude less than in the simulations. Thus it is expected that a value of 0.15 is an upper bound to the difference between the value of  $D_\alpha$  obtained from the projected vs. the 3-D structure.

For soot agglomerates in the size range 5.5–12  $\mu\text{m}$ , we obtain  $\bar{D}_\alpha = 1.82$  based on five agglomerates. This is to be compared with an average value of 1.90 based on the Langevin trajectory method and also a value of 1.90 reported by Meakin<sup>23</sup> for random linear trajectories. So the difference between the values of  $D_\alpha$  given above is within the uncertainty associated with the experiments and the simulations.

Our analysis of soot agglomerates indicates that the power law behavior is observed only over one-third to two-thirds of the total range in  $\log r$ . This may present a severe limitation to describing soot agglomerate properties such as the light extinction coefficient and friction force based on a fractal structure. Of course, it is the pair correlation function based on 3-D coordinates that is the quantity of interest, and the computer simulations in this study (see Figure 13) indicate that the power law range is significantly greater based on 3-D coordinates. In the simulations described above, Meakin<sup>9</sup> found no well-defined power law region for  $c(r)$  for the projected cluster; while for the 3-D coordinates, a power law behavior over

a decade in the radius was found. Since periodic boundary conditions were used in Meakin's computation of  $c(r)$ , the exponential falloff at large particle size is not obtained. Further experimental work on the 3-D coordinate structure of agglomerates and of the properties of size-classified soot agglomerates is necessary to determine the utility (and validity) of a fractal description of soot. Knowledge of the pair correlation function is important for describing soot agglomerate properties regardless of their fractal (or nonfractal) structure.

It was mentioned in the previous section that  $D_\alpha$  for clusters with overall size  $> 12 \mu\text{m}$  was about 0.1 larger than for agglomerates between 5.5 and 12  $\mu\text{m}$ . It is even possible for these clusters that  $D_f > 2.0$ , since this analysis technique breaks down as  $D_f$  approaches 2.0. A decrease in digitization resolution was dismissed as an explanation for this increase in  $D_f$ . It is possible that surface forces at a single contact point linking clusters may not be adequate to maintain the agglomerate's structure. As a consequence, restructuring of clusters to form denser, more stable agglomerates may become likely.

In order to compare the results of this structural analysis to the results obtained by Schaefer et al.<sup>10</sup> for carbon black, information is needed in regard to the cluster distribution. We observe an apparent dependence of the effective dimensionality on the cluster size. For cluster sizes in the range 5.5–12.0  $\mu\text{m}$ , a value of  $\bar{D}_\alpha = 1.82$  is determined. In general, however, such large clusters have not been observed for TEM samples collected from carbon black suspensions in liquids. It is not clear whether fractal character would be observed in light scattering experiments with small agglomerates.

Forrest and Witten's<sup>5</sup> pioneering experimental study of Fe, Zn, and  $\text{SiO}_2$  agglomerates provided the basis for the extension of such work to soot agglomerates as presented in this paper. Comparably sized soot agglomerates were determined to have  $D_\alpha$  similar to the value obtained by Forrest and Witten (1.7–1.9). The pair correlation function analysis in this study provides information not only where power law relationships are observed but also where exponential behavior predominates. To accomplish this the entire agglomerate structure was evaluated, as opposed to certain internal regions.

**Acknowledgment.** We acknowledge the work of Eric Steel of the NBS Microanalysis Group in performing the TEM analysis, Dr. David Bright for the development and use of the image processing methods discussed in the paper, and Dr. Raymond Mountain, NBS Center for Chemical Engineering, who performed the computer simulations for the agglomerate growth. This research was supported by the NBS Cooperative Research program and by the Defense Nuclear Agency.

(23) Meakin, P. *J. Colloid Interface Sci.* 1984, 102, 505.